



## City Research Online

### City, University of London Institutional Repository

---

**Citation:** Tamanna, N., Crouch, R.S. & Naher, S. (2019). Progress in Numerical Simulation of the Laser Cladding Process. *Optics and Lasers in Engineering*, 122, pp. 151-163. doi: 10.1016/j.optlaseng.2019.05.026

This is the accepted version of the paper.

This version of the publication may differ from the final published version.

---

**Permanent repository link:** <https://openaccess.city.ac.uk/id/eprint/22286/>

**Link to published version:** <https://doi.org/10.1016/j.optlaseng.2019.05.026>

**Copyright:** City Research Online aims to make research outputs of City, University of London available to a wider audience. Copyright and Moral Rights remain with the author(s) and/or copyright holders. URLs from City Research Online may be freely distributed and linked to.

**Reuse:** Copies of full items can be used for personal research or study, educational, or not-for-profit purposes without prior permission or charge. Provided that the authors, title and full bibliographic details are credited, a hyperlink and/or URL is given for the original metadata page and the content is not changed in any way.

---

---

---

City Research Online:

<http://openaccess.city.ac.uk/>

[publications@city.ac.uk](mailto:publications@city.ac.uk)

---

# Progress in Numerical Simulation of the Laser Cladding Process

Nusrat Tamanna<sup>a</sup>, Roger Crouch<sup>a</sup> and Sumsun Naher<sup>a,\*</sup>

<sup>a</sup> City, University of London, Northampton Square, London EC1V 0HB, United Kingdom

\* Corresponding author: [sumsun.naher.1@city.ac.uk](mailto:sumsun.naher.1@city.ac.uk)  
Orcid ID: [orcid.org/0000-0003-2047-5807](https://orcid.org/0000-0003-2047-5807)

## Abstract

Laser Cladding is one of the developing manufacturing techniques used for diverse applications such as coating, repairing and prototyping. Complex processing phenomena and the formation and growth of thin clad of few micrometers to millimeters range in most cases are yet to be fully understood. However, in recent past, several numerical models have been reported to get some understanding of physical, dynamic and metallurgical phenomena of this process. This article reviews the progress of numerical simulations spanning over three distinct stages of the process to model powder flow dynamics, melt pool and clad properties. For each stage, the governing equations, the effect of process variables and experimental validation techniques have been discussed. Specifically, we have outlined some of the underlying assumptions in the current numerical models which can act as pointers for further improvement of the existing numerical models. Authors recommend that numerical simulation results have to be complemented with experimental results to achieve better clad properties.

**Keywords:** Laser Cladding; numerical simulation; powder flow dynamics; melt pool; clad properties

# Contents

<b>1. Introduction</b> .....	3
<b>2. Powder flow dynamics</b> .....	7
<b>2.1 Modelling of powder flow characteristics</b> .....	9
2.1.1 Powder-nozzle interaction zone .....	9
2.1.2 Powder-laser interaction zone.....	11
2.1.3 Powder-substrate interaction zone.....	12
<b>2.2 Experimental validation</b> .....	15
<b>3. Melt pool</b> .....	17
<b>3.1 Heat transfer in melt pool</b> .....	17
<b>3.2 Melt pool geometry and shape</b> .....	20
<b>3.3 Fluid flow in melt pool</b> .....	21
<b>3.4 Experimental validation</b> .....	25
<b>4. Clad properties</b> .....	27
<b>4.1 Modelling clad properties</b> .....	27
<b>4.2 Experimental validation</b> .....	31
<b>5. The relevance of laser cladding processes in additive manufacturing</b> .....	33
<b>6. Future outlook</b> .....	37
<b>7. Conclusion</b> .....	40
<b>Acknowledgments</b> .....	44
References.....	45
List of Figures.....	64
List of Tables.....	64

## 1. Introduction

Low heat input, high solidification rate, excellent metallurgical bonding, deposition of functionally graded materials as well as rapid prototyping with homogenous structure made Laser Cladding (LC) a unique thermal coating process [1]. In the LC process, a laser heat source is utilized to deposit a thin layer (0.05-2 mm) of metal/ceramic, known as clad, on a solid substrate ranging from  $\mu\text{m}$  [2] to mm [3]. In the late 1970's, a clad was achieved by preplacing a layer of ceramic powders on a metallic substrate and melting these preplaced powders by using a laser heat source [1]. Almost a decade later in 1980, W. M. Steen and V. Weerasinghe introduced another process where powders are conveyed through a nozzle to the surface of substrate [1,4]. Concurrently, this process received an attention from the turbine manufacturing industry, where they started using it for hard-facing of turbine blade. Since then, the LC process is being used in various material processing industries for coatings [5], repairing [6], rapid prototyping [7] and making complex shapes.

In the LC process, the feeding of cladding materials can be performed using different methods. Depending on the ways of feeding, the LC process can be categorised into four types: preplaced powder system [8,9], coaxial powder system [10,11], off axis powder system [12] and wire feeding system [13,14], as shown in Fig. 1. Fig. 1 (a) shows the preplaced powder system. As the name suggest, powders are pre-placed on the substrate before applying the laser heat source. In the coaxial powder system, powders are delivered along the same axis (co-axially) of the laser beam, as shown in Fig. 1 (b). Fig. 1 (c) shows the schematic of off-axis powder system where powders are conveyed to the melt pool by a nozzle which is off axis to the laser beam. In the wire feeding system, wire is used as cladding material instead of powders, as shown

in Fig. 1 (d). The typical size of powders range from 50 to 150  $\mu\text{m}$  [15,16] and the diameter of wire is around 1 mm [13].

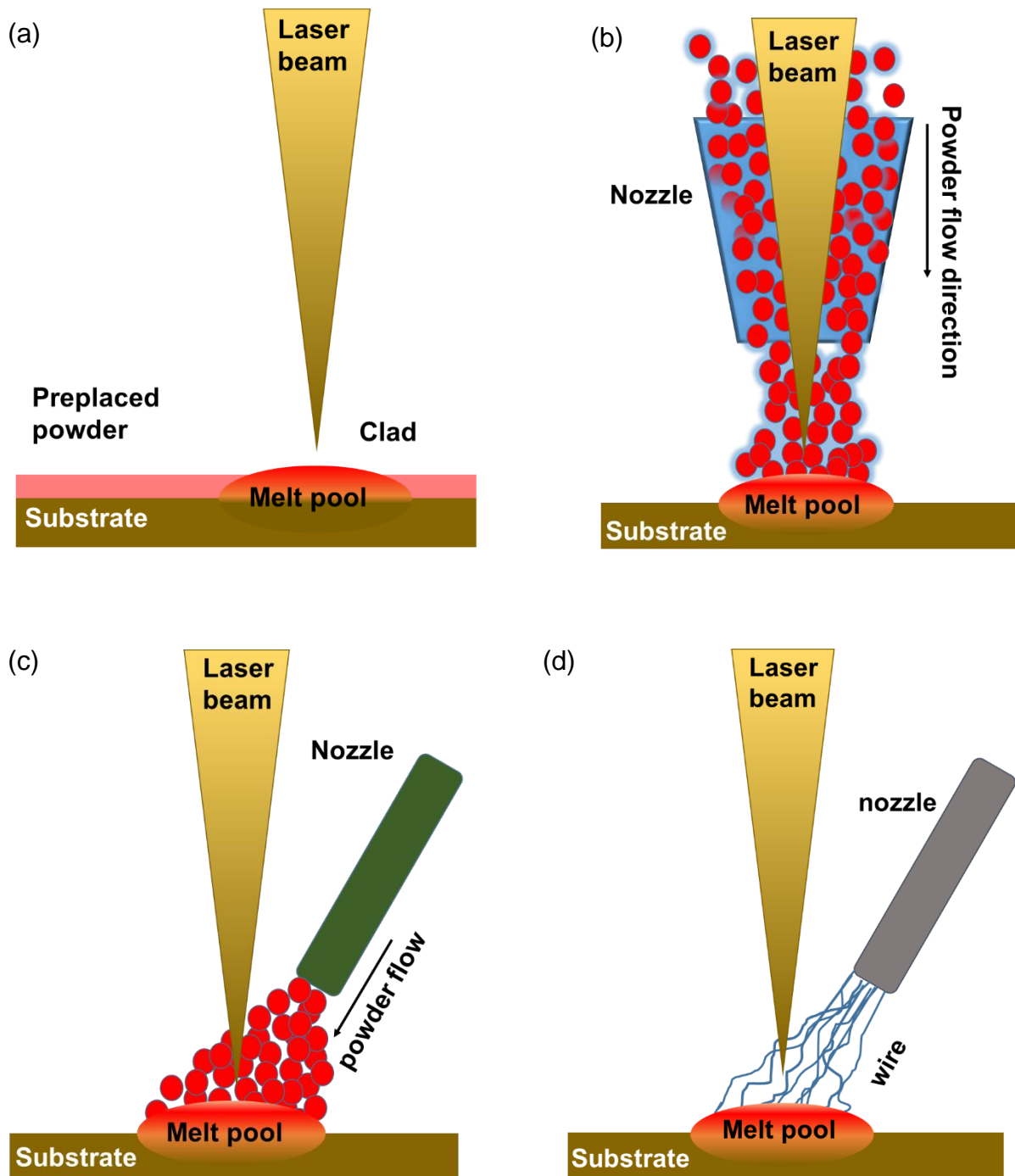


Fig. 1 Schematic diagrams of feeding system (a) preplaced powder system, (b) co-axial powder system, (c) off-axis powder system and (d) wire feeding system.

The coaxial LC process is more robust than other three feeding systems because it offers precise feeding rate in any direction. A 3D schematic diagram of a typical coaxial LC process is shown in Fig. 2 (a). In this process, a coaxial nozzle consists of powder feeder and laser system is moving in Z direction while powders are delivered along the Y axis. Coaxial nozzle moves with the laser beam at a certain scanning speed over a stationary substrate surface. A micrograph of laser cladded zone ( clad), heat affected zone (HAZ) and substrate is shown in Fig. 2 (b) [17]. These three layers can be easily distinguished from each other by their texture.

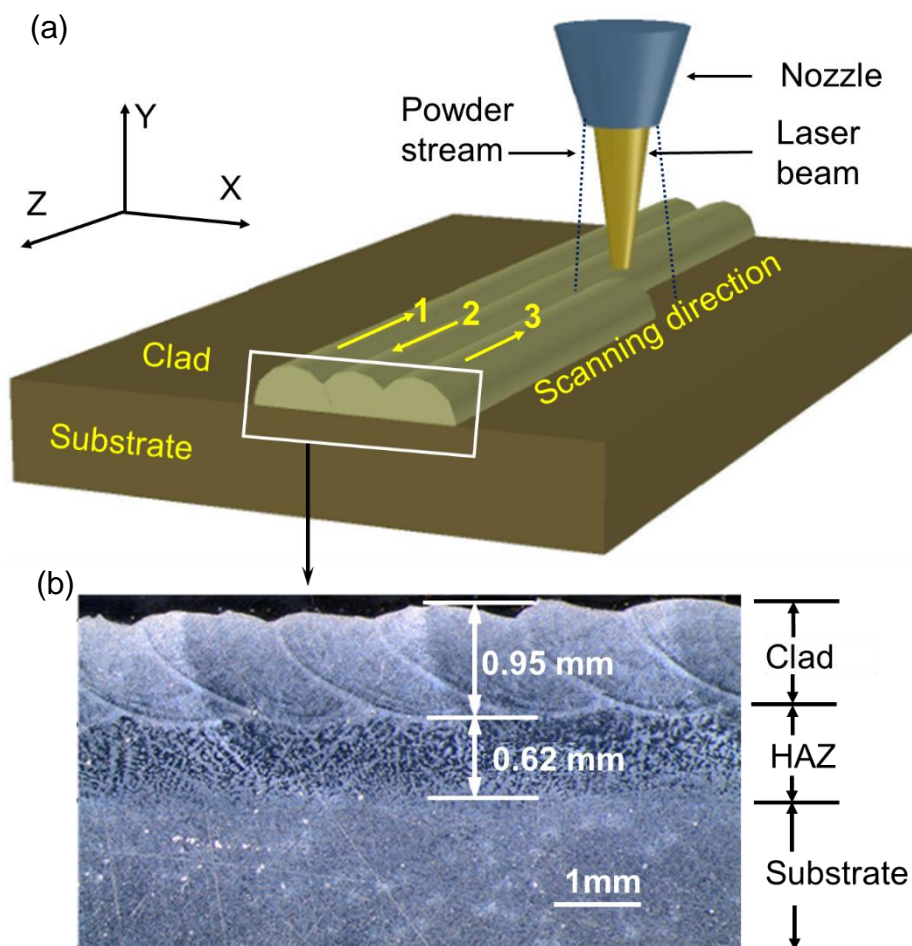


Fig. 2 (a) A schematic diagram of the coaxial Laser Cladding process, (b) micrograph, presenting deposited clad, HAZ and substrate area [17].

The LC process is carried out in three stages: powder flow dynamics, melt pool and clad properties. Complex phenomena such as powder flow behaviour, particle interactions with nozzle, laser and substrate, heat transfer and melt pool characteristics are difficult to understand from only experimental results. Therefore, several analytical models [18,19] and numerical simulations have been applied in three stages to understand those complex phenomena. To date, several reviews have been done on Laser Cladding process focused on experimental work [7,20,21]. However, to the knowledge of the authors there is no published work that only focused on the review of simulation work of LC process. Therefore, this review focuses on the development of the numerical modelling techniques which have been used to understand and predict the important features of the process physics and the coupling of different models. This review is divided into seven sections. In the first section, an overall idea about LC process is given. Section two to four are based on simulations that have been applied in three stages (powder flow dynamics, melt pool and clad properties). Section two consists of interactions of powder with nozzle, laser and substrate, powder flow characteristics, effect of process variables on powder flow and model validation. Section three comprises of heat transfer in the melt pool, melt pool geometry and shape, flow characteristics of melt pool, and model validation. After that, the clad properties include simulations of phase transformation, microstructure, hardness and residual stresses, presented in section four. This section also includes model validation for the prediction of hardness and residual stresses. Section five contains the relevance of laser cladding processes in additive manufacturing in relation to the simulation. After that, a future outlook of the LC process has been added in section six. Finally, section seven includes the conclusion and future prediction of LC process.

## 2. Powder flow dynamics

Powder flow dynamics is an important feature in the coaxial or the off axis powder feeding system as it can predict powder flow characteristics such as powder motion, powder flow profile, interactions of powder with laser system and thus used in optimization of process parameters. In these feeding systems, powders are carried by the drag force of the inert gas. Generally, the turbulent flow of carrier gas is considered as a continuum phase and hence solved using time averaged Navier-Stokes equations, whereas powders phase being dispersed in nature solved using Lagrangian equation [16,22–25].

The motion of gases were calculated using Eqs. 1-4 of conservation of mass [16,23,24] and momentum [16,22,23].

$$\nabla \cdot (\rho \mathbf{U}) = 0 \quad (1)$$

$$\partial/\partial t (\rho U) + \nabla \cdot (\rho \mathbf{U}U) = -\partial p/\partial X + \mu_l \nabla \cdot (\nabla U) + f \text{ in X direction} \quad (2)$$

$$\partial/\partial t (\rho V) + \nabla \cdot (\rho \mathbf{U}V) = -\partial p/\partial Y + \mu_l \nabla \cdot (\nabla V) + f \text{ in Y direction} \quad (3)$$

$$\partial/\partial t (\rho W) + \nabla \cdot (\rho \mathbf{U}W) = -\partial p/\partial Z + \mu_l \nabla \cdot (\nabla W) + f \text{ in Z direction} \quad (4)$$

where  $\rho$  is the density of gas,  $\mathbf{U}$  is the instantaneous velocity of gas field,  $t$  is time,  $U, V$  and  $W$  are the velocity component at  $X, Y$  and  $Z$  direction in turbulent flow,  $p$  is the pressure of gas,  $\mu_l$  is the dynamic viscosity of gas and  $f$  is the external force acting on gas. In this method, gas is assumed as incompressible fluid.

The motion of powder particles is calculated using Eq. 5.

$$m_p dv_p/dt = A_p C_D \rho_p / 2 (\mathbf{u} - v_p) |\mathbf{u} - v_p| + m_p g \quad (5)$$

where  $m_p$  the mass of a particle is,  $v_p$  is the velocity of particle,  $A_p$  is the area of particle,  $C_D$  is the drag coefficient,  $\rho_p$  is the density of the particle and  $g$  is the gravity force. To solve this equation, powders are assumed as solid,

spherical and chemically homogenous. Moreover, the collision between particles are ignored.

Furthermore, if powders while travelling from the nozzle exit to the substrate intersect the laser beam path, they absorb heat from the laser heat source. The transfer of heat from laser beam to powders is governed by Eq. 6.

$$\frac{1}{3} r_p \rho_p C_p \frac{dT}{dt} = \frac{1}{4} (I_{dir} + I_{ref}) \eta_p - h(T - T_\infty) - \varepsilon \sigma (T^4 - T_\infty^4) - \frac{1}{3} a \rho L_f \Gamma_p \frac{1}{dt} \quad (6)$$

where  $r_p$  is the radius of particle,  $\rho_p$  is the density of the particle,  $C_p$  is the specific heat of powder,  $I_{dir}$  and  $I_{ref}$  are the energy coming from laser beam on the particle and reflected from substrate respectively,  $\eta_p$  is the absorption coefficient of particle,  $h$  is the heat convection coefficient,  $T$  is the temperature of particle,  $T_\infty$  is the temperature of the surrounding gas,  $\varepsilon$  is the particle emissivity and  $L_f$  is the latent heat of fusion. Here, the temperature gradient within particles are negligible as the biot number is less than 0.001. These equations are generally solved by computational fluid dynamic (CFD) technique using commercial software packages like CFD-ACE, CFD fluent and ANSYS fluent.

## 2.1 Modelling of powder flow characteristics

The characteristics of the powder flow is affected by interactions of powders with nozzle, laser irradiance and substrate. Therefore, based on these interactions, the simulation of entire powder flow is carried out in three distinct zones namely powder-nozzle [26,27] powder-laser [16,28–31] and powder-substrate [16], shown by a, b and c respectively in Fig. 3.

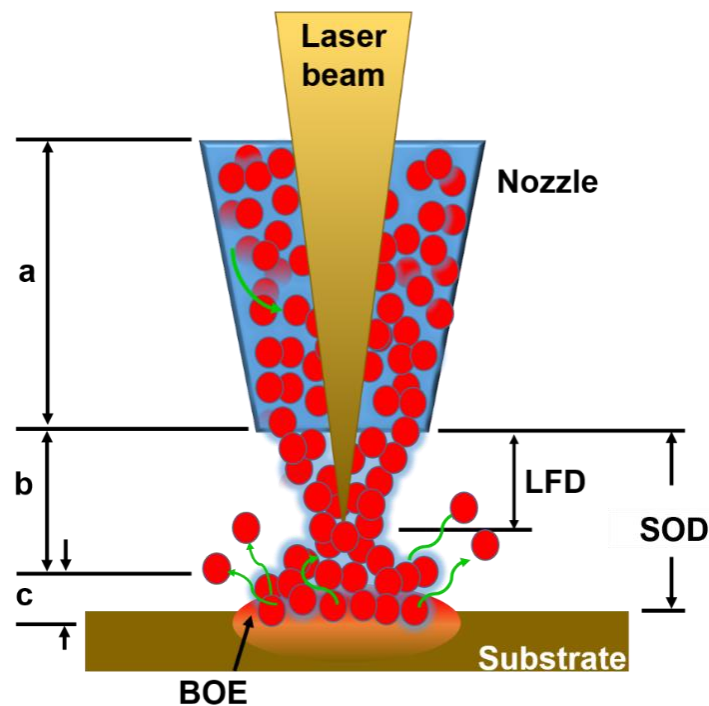


Fig. 3 Schematic diagram of several interaction zones along the laser beam to substrate. The interactions can be divided into three zones such as (a) powder-nozzle [34,39], (b) powder-laser [22,39,41,43] and (c) powder-substrate [22]. LFD = laser focus distance, SOD = stand of distance, BOE = bounce off effect.

### 2.1.1 Powder-nozzle interaction zone

In powder-nozzle interaction zone, particles experience a collision with the walls of the nozzle as they are dragged by the carrier gas. Depending on the loss of energy of the particle on collision, two types of collisions have been described in literature, i.e. elastic and inelastic collision [27]. In the elastic collision, there is no energy loss whereas the energy loss takes place in the inelastic collision [32].

Powders coming from the nozzle exit form powder flow stream. Typically, powders flow expands at the exit of the nozzle due to gravity and flow of gases which merge into a convergence point after a certain distance, and diverge again. Therefore, the distribution of powder in the powder flow near the exit point of nozzle and at the convergence point is considered to be of annular and Gaussian shape respectively [24,25,33,34]. Nevertheless, the flow characteristics depend on nozzle geometry, shape and size of powders, environmental pressure and type of carrier gas. Nozzle geometry is one of the significant parameters which controls the flow characteristics [35,36]. The inward position of middle nozzle converge powders around 5 mm away from the nozzle exit whereas the outward position shift the converge point to 8 mm [35]. Additionally, the concentration of powder increased up to 50% by using outward position of middle nozzle [37]. The difference of nozzle angles also has impact on the concentration of powder in the distribution. Zhang et al. investigated the concentration of powders for three different nozzle angles. 45, 60 and 75 [38]. The maximum concentration of powders at the convergence point was achieved using 60° nozzle angle over 45° and 75° nozzle angles [38]. Another parameter is particle size which effect on the trajectory of the powders flow. For example, finer powders (less than 10  $\mu\text{m}$ ) were difficult to converge than coarse powders (more than 100  $\mu\text{m}$ ) [33], because the trajectory of finer particles easily shifted by gas flow than heavy particles. Moreover, the concentration of particle in the powder stream was lower in case of larger particle due to higher gravity force. Another study by Smurov et al. showed that the trajectory of coarse particle was more dispersed than finer particles due to the collision with the nozzle [27].

The shape of powders is considered spherical in most simulations but the non-spherical powders can alter the results of powder concentration in the distribution [37].

The results of simulation with non-spherical particles matched well with the experimental results whereas spherical powder overestimated the peak concentration value in powder flow [24,34].

The velocity of powders is affected by density and compressibility of carrier gas [38]. For example, the use of helium increased the velocity of powders over the argon due to its lower density and higher compressibility [38].

### **2.1.2 Powder-laser interaction zone**

In powder-laser interaction zone, due to the interaction between particle and laser beam, the laser energy gets attenuated by reflection, absorption, radiation and beam scattering. In literature, several models based on ray tracing procedure [29], shadow model [39], resolution model [40] and light propulsion force model [41,42] are reported to predict the attenuation of laser energy. Total heat transfer phenomena consists of energy absorption of particles from laser heat source, heat conduction in the powder and heat dissipation to the environment from the particle by convection and radiation. The internal conduction in powders is taken based on biot number [41–44]. Recently, liquid fraction evolution during the phase change under the laser irradiation has been considered [45]. The absorbed laser power increases temperature in the powder flow distribution which adds additional thermal energy to the melt pool. The energy balance equation for the temperature distribution of particle is given in Eq 6. The temperature distribution of powder flow is highly dependent on laser power [31] and the distance between the nozzle exit and the focal point of lens (marked as LFD in Fig. 3) [44]. The peak temperature of powders increased with increasing laser power. However, for very high laser power, particles tends to vaporise, thus causing approximately 25% reduction in powder mass [31]. LFD is one of the controlling factors of laser power

absorption. Therefore, by optimization of LFD, homogenous temperature in the distribution can be achieved which increases the deposition efficiency [44].

### **2.1.3 Powder-substrate interaction zone**

In the early stage of the simulation, the substrate was not considered in the simulation of powder flow [23]. The consideration of the position of substrate affects the powder flow characteristics. The distance between the position of the top surface of the substrate and the exit of the nozzle is called the stand-off distance (SOD) as shown in Fig. 3. Therefore, SOD has a significant effect in the interaction of powder and substrate [35]. For example, to produce high quality clad, the convergence point of powders should be equal to SOD [35]. Ibarra-Medina et al. showed that the higher concentration was obtained due to bounce off of particles from the substrate when the substrate was positioned near the nozzle exits [16]. The chronological development of the models in powder flow dynamics, their focus, model type, used software, clad/powder materials and assumptions have been summarized in Table 1.

Table 1: The chronological development of numerical models on powder flow dynamics for co-axial powder type.

Ref.	Focus of the work	Model type	Software used	Material (clad or substrate) / Size ( $\mu\text{m}$ ) / shape	Shortcoming in the model
Lin et al. [23] 2000	Simulated powder flow structure by varying arrangement of nozzle exit	2D	CFD FLUENT	Stainless steel / 45-105 / spherical	The collision among particles, the interaction of particles with nozzle wall and laser beam were ignored.
Pan et al. [37] 2005	Developed a numerical model of metallic powder flow with non-spherical powder considering interaction of powders with nozzle wall	3D	Not mentioned	Iron / 100 / non-spherical	No carrier gas was considered in the powder flow.
Zekovic et al. [22] 2007	Simulated a gas-powder flow using radially symmetrical nozzle	3D	FLUENT	H13 tool steel / 45-180 / spherical	The collision of particles and the interaction of particles with laser beam was ignored.
Wen et al. [24] 2009	Predicted a powder flow in and after the nozzle considering various particle morphology and size	3D	CFD FLUENT	Stellite 6 / 45-180 / non-spherical	Particles collision and laser attenuation were not considered.
Taberero et al. [33] 2010	Developed a general model for any kind of material considering powder feed rate and powder size	3D	CFD FLUENT	Stainless steel / 45-150 Inconel / 40-110 / spherical in both case	The interaction of powder with nozzle wall, laser beam and substrate are not considered.

Ibarra-Medina et al. [16] 2011	Developed a numerical model of powder flow considering interaction of powder with laser beam and substrate	3D	CFD-ACE+	Stainless steel / 53-150 / spherical	The collision of powder with nozzle wall was ignored. The carrier gas velocity, different kind of carrier gas and material effect were ignored.
Nie et al. [46] 2014	Predicted powder flow distribution considering various particle size	3D	ANSYS FLUENT	Inconel 718 / 50-200 / spherical	Model ignored the presence of substrate and energy loss due to interaction with wall.
Zhang et al. [38] 2016	Developed a powder flow to investigate environmental pressure ,vacuum effect and different carrier gas effect on the powder flow distribution	3D	ANSYS	Titanium / 50 / non-spherical	All kinds of interactions were ignored.
Kovalev et al. [32] 2017	Predicted a powder flow considering inelastic collision of particle with the nozzle wall for different substrate position	3D	FLUENT	Steel / 60 / spherical	The nozzle design, carrier gas parameters and collision between particles are ignored.

---

## 2.2 Experimental validation

In literature, predicted powder flow characteristics such as the maximum concentration of powders, the position of maximum concentration, the shape of powder flow from nozzle exit to substrate and velocity of powders have been validated experimentally using image capturing techniques.

The maximum concentration of powder in the flow was predicted considering non-spherical particle collision and nozzle wall roughness for various nozzle geometry such as inward middle nozzle, outward middle nozzle [37]. In experiment, light was used to illuminate powder particles at the vertical cross section of the powder flow and images were captured using a high speed camera. Then, object detection process was used to extract powders concentration from the captured images. Maximum 20% mismatch was observed between experimental and simulated results for outward middle nozzle. This mismatch was attributed to the difficulty in distinguishing the individual particle by image processing method, especially in the concentrated region where particles tend to overlap with their neighbour.

Zekovic et al. experimentally verified the position of maximum powder concentration [22]. The cylindrical pattern of the maximum powder concentration along the vertical axis in the SOD range was found from simulated results. Experimentally, powder concentration was determined by measuring the intensity of scattered light using a charged couple device (CCD) sensor. The measured result showed same range as obtained in simulation. CCD sensor was also used to measure powder distribution at different plane [33]. The experimental results showed an annular shape at the nozzle exit and Gaussian shape near the powder flow convergence plane which corresponded with simulation [33].

Balu et al. developed a model to predict the velocity of three different particles (NT-20, NT-80, and WC) at the nozzle exit and validated their simulated results experimentally [47]. A high speed CCD camera was used to measure the position of particle with time in the powder stream which was illuminated by a green laser of 532 nm wavelength. The simulated velocity of NT-20, NT-80, and WC was 8.98 m/s, 7.69 m/s and 7.19 m/s respectively whereas the measured velocity was 10.1 m/s, 8.48 m/s and 6.87 m/s respectively. In case of WC powder, the simulated velocity was higher than the measured value while other two cases showed opposite trend. However, the differences between the simulated and experimental results in all three cases were consistent.

### 3. Melt pool

Similar to the simulation of powder flow analysis, as discussed in previous section, the melt pool constitutes another discrete part of the entire process. It focuses on heat transfer [34,48–50], melt pool geometry, melt pool shape [51–54] and fluid flow velocity [24,34,48,50,55–57]. In order to predict these dynamic phenomena numerically, level set method [24,50,55,58,59], volume of fluid method [12,48,51,52,56,60–62], finite element method [10,63–68] and finite difference method [31] have been adopted in various commercial multi-physics platforms such as ANSYS, FLUENT, ANSYS-CFD, ABAQUS and COMSOL. This section gives the overview of development in simulation to predict aforementioned parameters of melt pool and experimental validation techniques.

#### 3.1 Heat transfer in melt pool

The first step in simulating temperature distribution in melt pool is to define the laser heat source which can be generally categorised in two types: pulse or continuous. The equations applied in simulation for pulse [66] and continuous [17,69] laser heat source as surface heat flux are defined in Eqs. 7-8.

$$\text{Pulse, } Q_{(x,y)} = P/\tau_t \pi R^2 \exp(-2r^2/R^2) \quad (7)$$

$$\text{Continuous, } Q_{(x,y)} = \eta P/\pi R^2 \exp(-2r^2/R^2) \quad (8)$$

where  $Q$  is the laser heat source,  $P$  is the laser power,  $\tau_t$  is the pulse duration,  $R$  is the radius of laser beam,  $\eta$  is the absorptivity of laser power and  $r$  is the radial distance from the centre of laser heat source.

In simulation, laser heat source was similarly applied as volumetric heat source [63] what is expressed in Eq. 9.

$$\text{Continuous, } Q_{(x,y,z)} = 6\eta P / \pi \sqrt{\pi} R^3 \exp(-3r^2/R^2)$$

(9)

where  $Q$  is the laser heat source,  $P$  is the laser power,  $R$  is the radius of laser beam,  $\eta$  is the absorptivity of laser power and  $r$  is the radial distance from the centre of laser heat source.

In literature, predominantly the Gaussian heat source [35,63,65,70–75] is used. However, Tseng et al. developed another heat source named tailor heat source considering the physical characteristics of laser source such as beam diameter, wave length, mode and focusing length [76]. The application of tailor heat source induced high intensive energy which produced high temperature in clad and substrate. The transient temperature distribution was predicted using conduction while convection and radiation were applied as boundary conditions. The conduction equation of laser heat source of this process can be seen in Eq.10.

$$\partial(\rho C_p T) / \partial t + \nabla \cdot (\rho C_p \mathbf{u} T) = \nabla \cdot (k \nabla T) + Q_{laser} \quad (10)$$

where  $\rho$  is the density of gas,  $C_p$  is the specific heat capacity,  $\mathbf{u}$  is the velocity of laser head,  $k$  is the thermal conductivity,  $\partial T$  is the particle temperature variation in the time  $\partial t$  and  $Q_{laser}$  is the heat flux from laser heat source.

Heat transfer simulations are mainly done in preplaced and coaxial powder system. The temperature distribution in both cases depends on laser heat source characteristics such as laser power, scanning speed, beam diameter, heat source mode and focusing point of beam. The additional investigated process parameters are powder bed thickness and feed rate for preplaced and coaxial powder system respectively.

In preplaced powder process, heat source was directly applied on the surface of preplaced powder [65]. Guo et al. studied the effect of laser power for proper melting of cladding material and certain portion of the substrate [64]. According to authors, below 240 W laser power, the clad could not form due to the lack of fusion whereas above 530 W laser power, material vaporized leading to poor clad quality. Moreover, laser power also controls dilution rate in the system. The dilution was increased from 6.25% at 2500 W to 33.75% at 3000 W which is detrimental for the clad [74]. The desirable dilution is around 3-8%. Another model showed that the effect of heat source on the peak temperature. The predicted peak temperature for TEM<sub>00</sub> Gaussian mode, a TEM<sub>01</sub> single mode and a tailored TEM<sub>mixed</sub> multi-mode were 7115°C, 3108°C and 2191°C respectively due to the different concentration of energy in the heat distribution [76]. The effect of powder bed thickness on the melt pool area was studied. It was observed that with increasing thickness of powder bed, area of melt pool increased while height decreased [77].

In the coaxial powder system, powder flows along the same axis of the laser heat source. Therefore, models for the coaxial feeding system use birth and kill technique to deposit clads. In birth and kill technique, elements must be killed in the clad area before applying any heat source and then deactivated elements remained in the process with near zero conductivity. When the heat source was applied on a specified location of the surface, the killed elements on that position in the clad area were activated. Using this technique, Hao et al. developed a finite element model (FEM) to simulate the temperature distribution [63]. This model was capable to predict temperature distribution with varying laser power, laser scanning speed and powder feed rate. Another study showed that increment of laser power (500 W) increased the temperature by 249°C [78]. Farahmand et al. reported a model to calculate cooling

rate varying the preheating temperature of the substrate [79]. Though, the peak temperature was increased with increasing the preheating temperature of the substrate, more stable melt pool was obtained because of slower thermal gradient. The addition of clad layer also increased the peak temperature of melt pool [17,54,80]. The same phenomenon was observed for the deposition of overlapped clad [48] and double track deposition [81]. All the models mentioned above did not consider the effect of fluid flow, interaction of powders and substrate on the melt pool temperature.

### **3.2 Melt pool geometry and shape**

The melt pool geometry and shape were predicted from temperature distribution profile and analytical functions of melt pool shape respectively. The typically used functions in literature are elliptical cylinder function [79,80], circular arc [82] and parabolic shape function [54] which calculate the melt pool boundary. The parameters that influence the geometry and shape of the melt pool are laser-powder interaction time, laser power, powder catchment efficiency, powder feed rate and laser scanning speed. The melt pool width and depth were found to increase with increasing the interaction time with laser beam [48,53,54] and laser power [10,13,48,49,53,54]. On the other hand, the resulted clad height was relatively constant with increasing the laser power [48,83]. Partes et al. [15] and Ya et al. [54] predicted the melt pool geometry by taking into account of laser power and powder catchment efficiency. Moreover, the increment of powder catchment efficiency changed the heat conduction process which altered the shape of the melt pool [84]. Both height and width increased with increasing feed rate in the process [10,13,55,56] while an opposite phenomenon was observed with increasing the laser scanning speed [10,55,60,85]. More importantly, the roughness of the melt pool surface also depends on process parameters. It was reported that the

lower laser power, lower scan speed, lower temperature of particle and substrate produced a smoother clad surface [60].

### 3.3 Fluid flow in melt pool

Marangoni force, the injected powders force and angle of melt pool surface determine the pattern and direction of molten fluid [34,48,55]. Surface tension between molten fluid and air is the origin of Marangoni force [57,86]. This Marangoni force transports the molten fluid from the laser centre point to the periphery of the melt pool, and consequently, form vortex in the melt pool [34,52,55]. Subsequently, the velocity of fluid decreased when molten fluid enter to the mushy zone due to the lower mobility of atom [34]. The addition of injected powder force with Marangoni force in coaxial powder feeding system increased the number of vortex, decreased the size of melt pool and changed the direction of fluid flow from the periphery to inward direction [51,55,56]. Since the fluid flow turned to inward direction from the surface, facilitated the transportation of the higher energy fluid to the bottom of the melt pool and increased melt pool depth. The fluid flow behaviour became more complicated during the deposition of multi-layer clad [48,58,61]. In this process, as cladding material was deposited on the top of the deposited clad, the angle between surface and clad was decreased. Lee et al. reported that with increasing the number of layers, the angle decreased at the top surface resulting lower velocity at the top layer melt pool [48]. The reported surface velocity decreased from 8.59 cm/s at first layer to 5.05 cm/s at third layer. The liquid flow is considered as incompressible Newtonian with laminar flow [52]. The governing equations of conservation of mass and momentum to solve the fluid flow in melt pool are given in Eqs. 11-14 .

$$\partial/\partial t (\rho) + \nabla \cdot (\rho \mathbf{V}) = 0 \quad (11)$$

$$\partial/\partial t (\rho u) + \nabla \cdot (\rho \mathbf{V} u) = \nabla \cdot (\mu_l (\rho/\rho_l) \nabla u) - \partial p/\partial X - (\mu_l/N)(\rho/\rho_l)(u - u_s) + S_x \text{ in X direction}$$

$$\frac{\partial}{\partial t}(\rho v) + \nabla \cdot (\rho \mathbf{V}v) = \nabla \cdot (\mu_l (\rho/\rho_l) \nabla v) - \partial p / \partial Y - (\mu_l / N)(\rho/\rho_l)(v - v_s) + \rho g + S_y \quad \text{in Y direction} \quad (12)$$

$$\frac{\partial}{\partial t}(\rho w) + \nabla \cdot (\rho \mathbf{V}w) = \nabla \cdot (\mu_l (\rho/\rho_l) \nabla w) - \partial p / \partial Z - (\mu_l / N)(\rho/\rho_l)(w - w_s) + S_z \quad \text{in Z direction} \quad (14)$$

where  $\rho_l$  is the density of liquid material,  $\mathbf{v}$  is the velocity vector of liquid material,  $u$ ,  $v$  and  $w$  are velocity component of liquid material in X, Y and Z,  $u_s$  and  $w_s$  are the tangential velocity at free surface,  $v_s$  is the normal velocity at the free surface,  $g$  is the gravity force,  $S_x$ ,  $S_y$  and  $S_z$  are the source of momentum per unit volume per unit time in X, Y and Z direction. In this method, fluid in melt pool was considered as compressible. Materials were assumed chemically homogenous and powders were assumed molten at the time it entered in the molten pool. Additionally, laser beam was assumed to be a Gaussian distribution.

The progress of simulation of thermal models to date have been summarized in Table 2. The contents of this table are the focus of work, applied methodology, materials used as clad and substrate.

Table 2. Chronological development of thermal model in melt pool

Ref.	Focus of work (method)	Material	Shortcomings in model
		Substrate / Clad	
Hoadley et al. [69]1992	Developed a thermal model to determine the temperature distribution considering the effect of laser power and laser scanning speed (in house coding)	Mild steel / cobalt based alloy	This model was restricted to two dimension.
Guo et al. [64] 2003	Simulated temperature profile considering the contact resistance between powder bed and the substrate (FEM)	ZM51 magnesium alloy / Al-12%Si alloy	The thermal properties of materials were considered constant even at high temperature.
Palumbo et al. [87] 2004	Predicted the temperature distribution in ring geometry (FEM)	Aluminium / copper alloy	A gap elements were added at the interface of the clad and substrate to adjust the dilution.
Choi et al. [56] 2005	Developed a 2D thermal model considering solidification, melting and evaporation phenomena of materials	Mild steel / H13 tool steel	Material properties were temperature independent.
Lei et al. [74] 2010	Developed temperature distribution of composite material (FEM)	Ti6Al4V / TiC-NiCrBSiC	The effect of latent heat, convection of liquid metal and temperature dependent composite material properties were ignored.
Holfman et al. [12] 2011	Developed a thermal model to predict the geometry of melt pool	Stellite 12 / mild steel	The melt pool flow was not considered.
Cheikh et al. [73] 2012	Developed a thermal model to predict the clad geometry (FEM)	Low carbon steel / 316L stainless steel	Material properties were accounted using Heaviside function.
Tseng et al. [76] 2013	Predicted the transient temperature distribution using a tailor heat source can be applied to other laser materials process simulation (FEM)	Medium carbon Steel S45C / cobalt based stellite 6	The fluid flow effect on the temperature distribution was not accounted.
Hao et al. [63] 2013	Simulated the temperature distribution using an inverse modelling approach (FEM)	Ti6Al4V / Ti6Al4V	The chemical reaction and fluid flow effect on the temperature distribution was not accounted.
Farahmand et al. [80] 2013	Developed a thermal model using top-hat power distribution (FEM) to predict temperature distribution	Mild-steel / AISI H13 powder	The chemical reaction between the materials was ignored.

Raju et al. [88] 2014	Predicted the temperature distribution varying laser scanning speed (FEM)	Nickel super alloy / Nickel super alloy	Phase transformation, latent heat of fusion and vaporization were not considered.
Nie et al. [46] 2015	Predicted the transient temperature distribution to calculate thermal cycles (FEM)	Inconel 718 / Inconel 718	The effect of convection of liquid metal was not considered in the thermal model.
Ya et al. [54] 2016	Developed a thermal model distribution taking into account of powder stream density and powder efficiency to predict the clad geometry (FEM)	DIN steel / Stellite 6	The clad geometry was calculated by the function of parabolic shape. The laser power should be reduced gradually to maintain the substrate temperature which was not considered.
Lee et al. [89] 2016	Predicted the temperature distribution for single and multi-layer clad (VOF)	IN718 / IN718	The peak temperature was restricted to liquidus temperature. Temperature dependent material properties was not used.
Masoomi et al. [90] 2017	Developed a thermal model using multi-laser system (FEM)	Ti6Al4V / Ti6Al4V	The wetting behaviour of liquid and solid, solid phase nucleation and pore generation were not accounted.
Nazemi at al. [91] (2018)	Used imposed thermal cycle (ITC) method to predict the temperature distribution.	AISI 1918 / P420 stainless steel	The fluid flow effect on the temperature distribution was not accounted.

### 3.4 Experimental validation

The simulations found in literature related to the melt pool dynamics mainly focused on the prediction of velocity of fluid flow, temperature distribution and dimension of melt pool. Out of these parameters, the measurement of the velocity of fluid flow in the melt pool is difficult due to its quick solidification process. The temperature distribution of the melt pool has been measured using pyrometers, thermocouple and micrographs. Pyrometers are used to measure the peak temperature and the temperature gradient on the surface from the thermal radiation of a heated object [92,93]. Kohler et al. used pyrometers to validate the simulated peak temperature [93]. In comparison to the predicted peak temperature (2424°C), the experimental result saturated at 1900°C due to the calibration limit of pyrometer. Another process to measure temperature distribution is using thermocouple. A type-K thermocouple, located 3 mm below the surface of substrate was used to record the transient temperature [94]. The results from experiments agreed well with the predicted results. Lei et al. validated the predicted temperature distribution from the SEM micrograph for the deposition of TiC/NiCrBSiC clad on Ti6Al4V substrate [74]. In this paper, based on the predicted temperature, authors divided the molten pool region in two separate areas called TiC melting area and TiC partially melting area. In TiC melting area, as the name suggests, the simulated temperature range (3140°C to 4200°C) was higher than the melting temperature (3140°C) of TiC. In TiC partially melting area, the predicted temperature range (from 1668°C to 3140°C) was above the melting temperature (1668°C) of NiCrBSi and below the melting temperature (3140°C) of TiC. Therefore, in TiC partially melting area, NiCrBSi was melted but the TiC was partially dissolved. The cross section morphology of a single clad track in the SEM micrograph showed precipitated TiC particles and dendrites in TiC melting section and

undissolved TiC particles in TiC was partially dissolved section. The observation of microstructure confirmed the temperature distribution obtained from simulation.

In order to validate the shape of the melt pool, micrographs of clad had been used. Y. Lei et al. validated the predicted depth of melt pool (0.76 mm) with the micrograph of the clad which showed 0.8 mm depth of melt pool [74]. In another work, Hofman et. Al used CCD camera and image processing technique to capture the real time dimension of the melt pool [12]. The simulated width and length were 2.77 mm and 3.92 mm respectively while the measured width and length were 2.98 mm and 3.96 mm. Simulation and experimental results showed good agreement.

## 4. Clad properties

This section reviews the simulation to predict properties of clad such as phase transformation, microstructure, hardness, residual stresses, and finally the experimental procedures to validate the simulation results.

### 4.1 Modelling clad properties

The simulation of clad properties are performed in conjunction with thermal model. In literature, two types of phase transformations are mentioned: diffusional phase transformations and diffusionless phase transformations [95]. In case of diffusional phase transformations, Johnson-Mehl-Avrami equation was used while diffusionless phase transformations is coded with Koinstinen-Marburguer equation [95]. Both of the equations are used for the non-isothermal phase transformation. Johnson-Mehl-Avrami equation is defined as in Eq 15.

$$f' = 1 - \exp(-mt^n) \quad (15)$$

where  $f'$  is the volume fraction of the new phase,  $m$  is a coefficient dependent on the temperature, composition of parent phase, and grain size  $t$  is the isothermal time duration and  $n$  is a coefficient dependent on the type of phase transformation and grain growth.

The expression of Koinstinen-Marburguer equation is given in Eq 16.

$$f'' = 1 - \exp(-c(M_s - T_\beta)) \quad (16)$$

where  $f''$  is the instantaneous volume fraction of the new phase, the value of  $c$  is 0.003,  $M_s$  is the martensitic transformation temperature and  $T_\beta$  is the beta transus temperature.

For non-isothermal phase transformation, Johnson–Mehl–Avrami–Kolmogorov equation was used to predict the fraction of crystallized volume [96], expressed as

$$f'''(T(t)) = 1 - \exp \left\{ - \left( \int_{t_0}^{t_e} K(T(t)) dt \right)^e \right\} \quad (17)$$

where  $f'''$  is the volume fraction of the new phase for non-isothermal phase transformation,  $t_0$  and  $t_e$  are initial and end time of phase transformation,  $K$  is the temperature dependent crystallization rate,  $t$  is the phase transformation time duration and  $e$  is the the dimensionality of growth of phases.

The solidification of dendritic microstructure has been simulated based on Kurz-Fisher and Trivedi theory [97]. It was shown that the rate of solidification increased with increasing cooling rates till it reached the critical value. Beyond the critical value of the cooling rate, the growth of nuclei hindered due to the inability of atom to diffuse. Therefore, the growth of nuclei become slower even at higher cooling rate [97]. In another work, the effect of process variables on the cooling rate was studied [98]. For example, with increasing the laser scanning speed, cooling rate decreased. Aditinnaly, It was observed that lower cooling rate produced smoother clad surface [59].

Hardness of clad can be predicted by coupling Thermo-kinetic relation with the thermal model [99,100]. In this model, the volume fraction of phases after thermal treatment and the hardness of each phases are required. The volume fractions of phases are calculated from the phase diagram, the cooling temperature from the thermal model and hardness of each phases are taken from the literature to calculate the hardness of total volume. The estimation of hardness through nanoindentation process was reported by Gu et al. [101]. They developed a FEM model of nanoindentation on particle to produce load vs displacement graph. From this graph,

depth of penetration was calculated, which is related with contact area of indenter. Finally, hardness was predicted from the applied load and the contact area.

In laser deposition process, residual stresses are generated in the deposited parts which causes the formation of crack and distortion. Therefore, prediction of residual stresses is an important area in simulation of the Laser Cladding process. Most of the simulations of predicting residual stresses in clad and substrate have been performed using finite element method [80,102–105]. In the early stage of simulation, elastic strain, plastic strain and thermal strain were considered to calculate residual stresses [17,103,106]. Later, phase transformation and volumetric strain increment were added in the calculation of residual stresses for more accurate analysis [80,107]. The governing equation to predict total strain, by assuming that there is no stress in the substrate before applying laser heat source is given eq.18.

$$\varepsilon = \varepsilon^{th} + \varepsilon^{el} + \varepsilon^{pl} + \varepsilon^{VV} + \varepsilon^{Trp} \quad (18)$$

where,  $\varepsilon^{el}$ ,  $\varepsilon^{pl}$ ,  $\varepsilon^{th}$ ,  $\varepsilon^{VV}$  and  $\varepsilon^{Trp}$  are elastic, plastic, thermal, volumetric and phase transformation strain respectively.

Strain is dependent on materials properties such as Young's modulus, Poisson ratio, yield strength and tensile strength. Few research groups used temperature independent material properties [106,108,109] while others used temperature dependent material properties for more accurate results [80,102,110].

In literature, residual stresses in normal direction and von Mises stresses have been predicted in single track, multi-tracks and overlapped clads. Mainly, tensile residual stresses were found in the clad area and small part of the substrate from the interface in single clad [102,106,111]. This tensile stress was balanced with the compressive stress inside the substrate. For practical applications, multi-tracks and overlapped

clads were deposited to observe the change of residual stresses [17,80,112]. In the multi-tracks deposition, maximum tensile stresses were located at the last track due to high cooling rate while it was reduced in previously formed track due to the relaxation of heat treatment [17,80]. In case of overlapped clad, the resistance of formation of cracks increased as the surface of previously formed clad got melted and decreased the tensile residual stresses [112].

The detrimental tensile residual stresses reduce the fatigue strength of the mechanical components by introducing cracks. Chew et al. have developed a model to predict fatigue life based on crack closure model [113]. This model estimated the fatigue life of the clad having multiple surface cracks.

## 4.2 Experimental validation

The predicted clad properties such as hardness and residual stresses have been experimentally validated. Hardness is usually measured using digital micro-hardness tester and nanoindenter whereas X-ray diffraction (XRD) is mainly used for residual stress measurement.

The simulated hardness was validated from the measurement of the digital micro-hardness tester (CLARK-700 AT) [100]. It calculated the Vickers hardness automatically from the diagonal length of indentation. The measured hardness showed a similar trend with the predicted hardness in the clad (from 671 HV to 649 HV) and the dilution zone (649 HV to 615 HV). In another study, the predicted hardness was validated from the results of a nanoindenter test [101]. This device, equipped with AFM, was used to measure the load and the displacement towards the indenter and into H13–TiC composite coatings. The hardness was calculated from the contact area and applied load. The measured and predicted hardness of TiC particle in the coating were  $30 \pm 5$  GPa and  $38.2 \pm 3.7$  GPa respectively. The hardness of H13 matrix was same around  $9 \pm 2$  GPa for both simulation and experiment.

In literature, the predicted residual stress has been predominantly validated using XRD [106,114]. In this method, the residual stress were calculated from a diffraction pattern and strain vs  $\text{Sin}^2\psi$  graph. The calculated stress from XRD at the clad top, at the interface and in the substrate were -300 MPa (compressive), 250 MPa (tensile) and -330 MPa (compressive) respectively. In comparison, the simulated stress at the clad top, at the interface and in the substrate were -290 MPa (compressive), 470 MPa (tensile) and -105 MPa respectively (compressive) [106]. The higher compressive stress at the interface, lower tensile stresses in the substrate and higher compressive stress on the clad surface were obtained in the XRD results. The reason of the

deviation could be attributed on two factors: (a) XRD provides an average value; (b) multiple clads were deposited on the same substrate.

## 5. The relevance of laser cladding processes in additive manufacturing

Additive manufacturing is a process of adding metal/ceramic/polymer materials layer by layer to produce three dimensional object. American Society for Testing and Materials (ASTM) classified this process into seven categories such as binder jetting, material extrusion, material jetting, sheet lamination, vat photopolymerization, powder bed fusion and direct energy deposition based on materials and machine technology [115,116]. The categories of additive manufacturing technology is shown in Fig. 4.

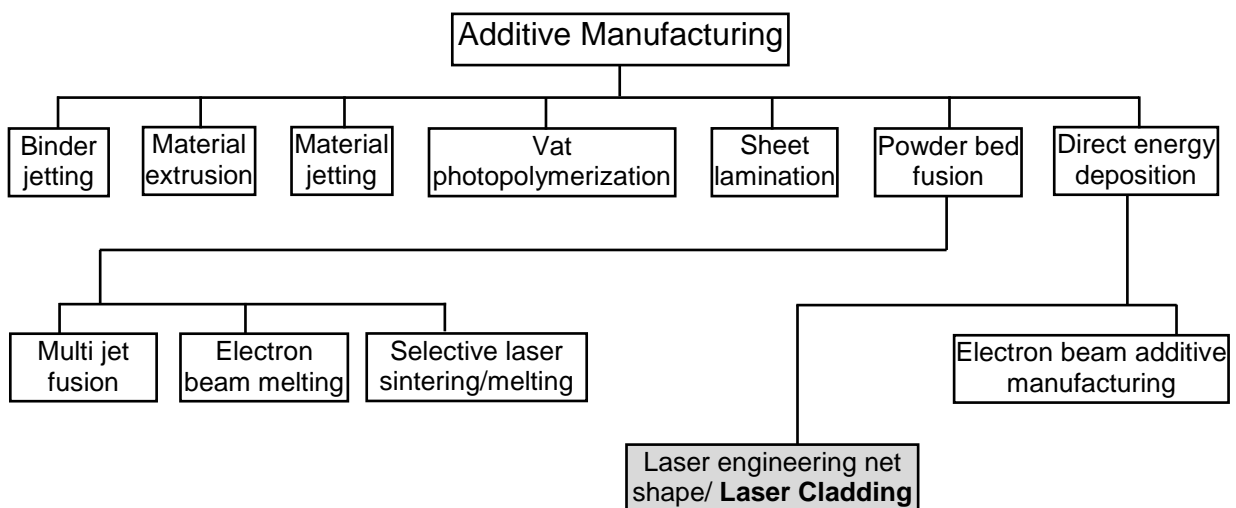


Fig. 4 The categories of additive manufacturing technology based on materials and machine technology [115,116].

In binder jetting, a thin layer of powder bed (polymer/metal/ceramic) is formed on the build platform [117]. Then a liquid binding agent is applied onto selected areas to create the bond between particles in that area. After finishing the first layer, build platform goes down to a defined height. After that, second layer of powders is spread on the build platform and binding agent is applied to create bond among particles. These steps keep repeated until the final/green part is achieved. Then the green part is separated from the loose powders followed by curing, debinding and sintering. In

material extrusion, molten or viscous materials (thermoplastic polymers, particulate composites, highly-filled polymers (HP) with metals or ceramics) are extruded through a nozzle/orifice to deposit stacked layers and subsequently a three-dimensional structure [118]. In material jetting technique, the droplets of liquid photosensitive material (photopolymer) are selectively deposited and solidified under ultraviolet (UV) light in successive layers [119]. In vat photopolymerization, a slurry is prepared by mixing powder materials (metal/ceramic) and photopolymer resin [120]. Then slurry is fed into the vat and the build plate is mounted in the vat. Next, a UV light is used to harden the slurry on the build plate selectively. After finishing first layer, build plate goes down to a defined height. These steps keep repeated until the final/green part is attained. Then excess slurry is removed and the green part is separated from the build part followed by debinding and sintering. In sheet lamination process, metal/composite sheet is placed on the cutting bed. A laser source is used to cut the material in a desired shape [121]. Then bonding between sheets is done by tape bonding/adhesive bonding/ tagging based on component and applications. Finally, trimming of the product is done if required. In powder bed fusion process, a thin layer of powder bed is formed on the build platform [122]. Then a focused thermal energy (laser/electron beam) is applied onto selected areas to sinter or melt/fuse powders. After that, second layer of powders is spread on the build platform and focused thermal energy is applied to create bond among particles. These steps keep repeated until the final component is achieved. Finally, loose powders are removed during post processing (machining, heat treatment). In direct energy deposition process, a focused thermal energy (laser/electron beam) is applied to melt the desired powder/wire material (metal/ceramics) which is conveyed by a nozzle and, finally deposits on an existing component for repair, coating, near net shape applications [123]. Similarly, Laser

Cladding process use focused laser heat source to melt powder/wire cladding material which is deposited in the melt pool of substrate material. Both processes have similar process steps such as transportation of powder (clad materials) through nozzle, melting powder particles using focused laser heat source and, finally depositing molten clad materials on the exiting substrate/component. Therefore, Laser Cladding is a significant relevance to laser additive manufacturing.

In Laser Cladding process, several empirical-statistical, analytical and numerical models have been done. These models are mainly used to predict geometries of clad, properties of clad, powder flow history and thermal profile, which can be applied in direct energy deposition process of additive manufacturing. The used method, process parameters and outcome of these models have been given in Fig. 5.

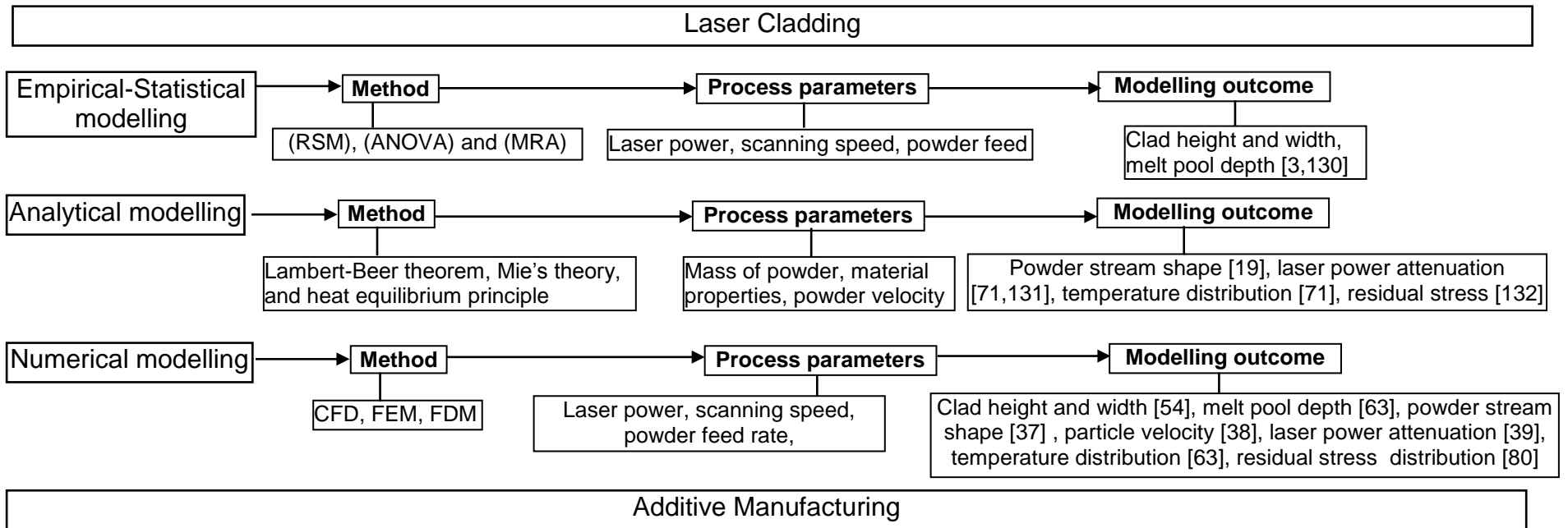


Fig. 5 Available models of the Laser Cladding process can be applied for additive manufacturing.

## 6. Future outlook

LC process offers use of a wide range of materials for coating, repairing, tooling, and rapid prototyping. Iron based alloy, titanium based alloy, cobalt based alloy, nickel based alloy, aluminium alloy, carbide, oxide, and nitride are already being used as cladding materials in industries [1]. Currently, bioactive glass is being used for biocompatibility of medical components [112]. High entropy alloy is used for oxidation and corrosion resistance [124]. Furthermore, deposition of composite coating (ceramic embedded metal matrix) is a recent trend to get high hardness and corrosion resistance using LC process. Therefore, this process has the capability to use a wide range of materials over conventional processes. Though this process has the capability to use of a wide range of materials, different material has different flow behaviour. Therefore, there is a high requirement to develop material feeding system for different type of materials. Additionally, the interaction between materials and laser (absorption, reflection and transmission) is a critical issue and not fully understood yet. The absorption of materials depends on the material properties and wavelength of laser. So, the research on materials properties, it's flow behaviour and it's interaction with laser will take place an important part in future research work.

Initially, LC process has been used to deposit cladding materials in millimetre level for coating or repairing in a single go. Recently, deposition of nano level coating (especially for particulate reinforced metal matrix composites) from nano sized powder is more prioritised as it provides outstanding ductility and fracture toughness compare to conventional micro-particulate reinforced metal matrix composites [125]. In order to achieve superior mechanical properties in the nano level coating, intensive research is going on using this process. So, this process is capable of producing coating with

fine micro-structure from nanometre to millimetre level for metal, ceramic and composite materials.

Both automated and manual laser cladding machines are available in the market. In the manual laser cladding machine, power setting, focusing distance, scanning speed, feeding of cladding materials, speed of cladding materials are set manually. This system takes a continuous attention of technical personnel to achieve good quality clad. Recently, automated refill of cladding materials and compact laser system are available. This system is capable to change diameter of laser beam and auto focus of laser system during cladding. However, easy transfer of laser beam to the treated zone, homogenous laser beam, developed sensor for tracking geometry of clad and solidification rate, in-depth knowledge on the behaviour of powders are under research in order to achieve fully automated system and high quality clad [126].

Conventional coating methods (arc welding and thermal spraying) have many drawbacks such as low desired outputs, difficulty in installation, high operational costs, requirement of large volume of heat and additional corrective machining. Thus, the operational costs and production time for these processes increased. However, the use of laser with focused and high power provides minimal design error, less production time and increased the efficiency of the LC process [127].

The goal of developing hybrid technology is to improve their individual advantages and minimize challenges. The development of hybrid technology is in the limelight in order to achieve high deposition rate, defect free and better mechanical properties of the components. For example, the laser induction hybrid cladding or Laser Cladding with induction preheating not only increases the laser energy efficiency (upto 64%), also produce crack free clad [128]. Furthermore, addition of ultrasonic vibration during

cladding can increase micro hardness in the clad, as it helps to refine grain and disperse the hard phase homogenously in the clad [129].

## 7. Conclusion

In this review paper, discretized numerical simulations of three stages of the Laser Cladding process have been summarized. Finite volume method has been mostly used to solve powder flow dynamics and fluid flow in melt pool, whereas, finite element method has been chosen to solve heat transfer and clad properties. Discretised models in all stages can be used to optimize the process parameters and explain the process physics as evident from their experimental validation. However, a complete model considering all stages and process parameters is still a complex procedure and far from the real status.

In comparison to large numbers of models pertaining to powder flow dynamics and melt pool stage, modelling in clad section is still limited. We need more robust models to predict various clad properties like hardness, residual stresses, wear resistance, phase transformation, microstructural evaluations etc. The modelling of post processes such as heat treatment, machining are need to be explored in detail.

Co-axial powder system is most widely investigated and attracted by industries for the final properties of the clad. However, the process is expensive as it requires additional process steps. There have been few modelling reported on preplaced powder system but modelling of remaining two feeding systems are still in nascent stage.

There has been good progress in numerical modelling of Laser cladding process in last decade, but few essential challenges has to be overcome before it can be fully adopted by other advanced manufacturing techniques such as laser based additive manufacturing.

<b>Nomenclature</b>	
$a$	It is a variable which takes the value 1 if T is melting temperature or 0 if T is different than melting point
$A_p$	The area of particle ( $m^2$ )
$C_p$	The specific heat (J/kg.K)
$C_D$	The drag coefficient
$\partial T$	The particle temperature variation in the time $\partial t$ (K)
$e$	The dimensionality of growth of phases
$f$	The external force acting on gas
$f'$	The volume fraction of the new phase
$f''$	Instantaneous volume fraction of the new phase
$f'''$	The volume fraction of the new phase for non-isothermal phase transformation
$g$	Gravity force ( $m/s^2$ )
$h$	The heat convection coefficient ( $W/m^2.K$ )
$I_{dir}$	The energy incident on the particle coming from the direct beam (J)
$I_{ref}$	The incident energy coming from substrate reflection (J)
$k$	Thermal conductivity ( $W/m.K$ )
$K$	A temperature dependent crystallization rate
$L_f$	The latent heat of fusion (J/kg)
$m_p$	The mass of a particle (kg)
$M_s$	The martensitic transformation temperature
$m$	A coefficient dependent on the temperature, composition of parent phase, and grain size
$N$	Permeability coefficient
$n$	A coefficient dependent on the type of phase transformation and grain growth
$P$	Laser power
$p$	The pressure of gas/liquid (Pa)
$Q_{laser}$	The heat flux from laser heat source ( $W/m^2$ )
$r$	The radial distance from the centre of laser heat source (m)
$r_p$	The particle radius ( $\mu m$ )
$R$	Radius of the laser beam ( $\mu m$ )

$S_x, S_y, S_z$	Source of momentum per unit volume per unit time in X, Y and Z direction
T	The temperature of the particle (K)
$T_\beta$	The beta transus temperature
$T_\infty$	The temperature of the surrounding gas (K)
$t$	The phase transformation time duration
$t_o$	Initial time of phase transformation
$t_e$	End time of phase transformation
<b>u</b>	Velocity of laser head (m/s)
$u, v, w$	Velocity component in X, Y and Z (m/s)
$u_s$	Tangential velocity at free surface (m/s)
$v_s$	Normal velocity at free surface (m/s)
$w_s$	Tangential velocity at free surface (m/s)
$v_p$	The velocity of particle (m/s)
<b>V</b>	Velocity vector (m/s)
<b>U</b>	Instantaneous velocity of gas field
U, V and W	Velocity component at X, Y and Z direction in turbulent flow
X, Y, Z	Cartesian coordinate (m)
$\nabla$	Vector differential operator/ grad operator
LFD	Laser focus distance
SOD	Stand of distance
BOE	Bounce off effect
Greek symbol	
$\varepsilon$	The particle emissivity
$\varepsilon^{el}, \varepsilon^{pl}, \varepsilon^{th}, \varepsilon^{\nabla V}, \varepsilon^{Trp}$	Elastic, plastic, thermal, volumetric and phase transformation strain respectively
$\eta$	The absorptivity of laser power
$\eta_p$	The absorption coefficient of particle
$\mu$	The molecular viscosity (kg/m.s)
$\mu_l$	The dynamic viscosity (kg/m.s)
$\rho_l$	Density of liquid phase (kg/m <sup>3</sup> )
$\rho$	The density of gas/clad/substrate material (kg/m <sup>3</sup> )
$\rho_p$	The density of the particle (kg/m <sup>3</sup> )
$\sigma$	The Stefan-Boltzman constant

$\tau_t$	Pulse duration (s)
----------	--------------------

## **Acknowledgments**

Thanks are addressed to EU funded Erasmus Mundus project, EM LEADERS [reference number: 551411-EM-1-2014-1-UK-ERA MUNDUS-EMA21\_EM], and School of Mathematics, Computer Science and Engineering of City, University of London. Authors are thankful to Md. Rahul Kumar for his support in reviewing and editing the manuscript.

## References

- [1] Toyserkani E, Khajepour A, F. Corbin S. Laser Cladding, 1st ed. USA: CRC Press; 2004.
- [2] Gabriel T, Rommel D, Scherm F, Gorywoda M, Glatzel U. Laser cladding of ultra-thin nickel-based superalloy sheets. *Materials (Basel)* 2017;10:1–12. doi:10.3390/ma10030279.
- [3] Sun Y, Hao M. Statistical analysis and optimization of process parameters in Ti6Al4V laser cladding using Nd:YAG laser. *Opt Lasers Eng* 2012;50:985–95. doi:10.1016/j.optlaseng.2012.01.018.
- [4] Mackwood AP, Crafer RC. Thermal modelling of laser welding and related processes: a literature review. *Opt Laser Technol* 2005;37:99–115. doi:10.1016/j.optlastec.2004.02.017.
- [5] Lin Y, Lei Y, Li X, Zhi X, Fu H. A study of TiB<sub>2</sub>/TiB gradient coating by laser cladding on titanium alloy. *Opt Lasers Eng* 2016;82:48–55. doi:10.1016/j.optlaseng.2016.01.016.
- [6] Wang W, Wang M, Jie Z, Sun F, Huang D. Research on the microstructure and wear resistance of titanium alloy structural members repaired by laser cladding. *Opt Lasers Eng* 2008;46:810–6. doi:10.1016/j.optlaseng.2008.05.015.
- [7] Liu J, Yu H, Chen C, Weng F, Dai J. Research and development status of laser cladding on magnesium alloys: A review. *Opt Lasers Eng* 2017;93:195–210. doi:10.1016/j.optlaseng.2017.02.007.

- [8] Farnia A, Malek Ghaini F, Sabbaghzadeh J. Effects of pulse duration and overlapping factor on melting ratio in preplaced pulsed Nd:YAG laser cladding. *Opt Lasers Eng* 2013;51:69–76. doi:10.1016/j.optlaseng.2012.07.015.
- [9] Muvvala G, Patra Karmakar D, Nath AK. Online monitoring of thermo-cycles and its correlation with microstructure in laser cladding of nickel based super alloy. *Opt Lasers Eng* 2017;88:139–52. doi:10.1016/j.optlaseng.2016.08.005.
- [10] El Cheikh H, Courant B, Branchu S, Hascoët JY, Guillén R. Analysis and prediction of single laser tracks geometrical characteristics in coaxial laser cladding process. *Opt Lasers Eng* 2012;50:413–22. doi:10.1016/j.optlaseng.2011.10.014.
- [11] Devojno OG, Feldshtein E, Kardapolava MA, Lutsko NI. On the formation features, microstructure and microhardness of single laser tracks formed by laser cladding of a NiCrBSi self-fluxing alloy. *Opt Lasers Eng* 2018;106:32–8. doi:10.1016/j.optlaseng.2018.02.004.
- [12] Hofman JT, De Lange DF, Pathiraj B, Meijer J. FEM modeling and experimental verification for dilution control in laser cladding. *J Mater Process Technol* 2011;211:187–96. doi:10.1016/j.jmatprotec.2010.09.007.
- [13] Hung C-F, Lin J. Solidification model of laser cladding with wire feeding technique. *J Laser Appl* 2004;16:140. doi:10.2351/1.1771167.
- [14] Kim J Do, Peng Y. Plunging method for Nd:YAG laser cladding with wire feeding. *Opt Lasers Eng* 2000;33:299–309. doi:10.1016/S0143-8166(00)00046-4.

- [15] Partes K. Analytical model of the catchment efficiency in high speed laser cladding. *Surf Coatings Technol* 2009;204:366–71.  
doi:10.1016/j.surfcoat.2009.07.041.
- [16] Ibarra-Medina J, Pinkerton AJ. A CFD model of the laser, coaxial powder stream and substrate interaction in laser cladding. *Phys Procedia* 2010;5:337–46. doi:10.1016/j.phpro.2010.08.060.
- [17] Chew Y, Pang JHL, Bi G, Song B. Thermo-mechanical model for simulating laser cladding induced residual stresses with single and multiple clad beads. *J Mater Process Technol* 2015;224:89–101.  
doi:10.1016/j.jmatprotec.2015.04.031.
- [18] Zhang Z, Farahmand P, Kovacevic R. Laser cladding of 420 stainless steel with molybdenum on mild steel A36 by a high power direct diode laser. *Mater Des* 2016;109:686–99. doi:10.1016/j.matdes.2016.07.114.
- [19] Huang Y, Khamesee MB, Toyserkani E. A comprehensive analytical model for laser powder-fed additive manufacturing. *Addit Manuf* 2016;12:90–9.  
doi:10.1016/j.addma.2016.07.001.
- [20] Weng F, Chen C, Yu H. Research status of laser cladding on titanium and its alloys: A review. *Mater Des* 2014;58:412–25.  
doi:10.1016/j.matdes.2014.01.077.
- [21] Quazi MM, Fazal MA, Haseeb ASMA, Yusof F, Masjuki HH, Arslan A. A Review to the Laser Cladding of Self-Lubricating Composite Coatings. *Lasers Manuf Mater Process* 2016;3:67–99. doi:10.1007/s40516-016-0025-8.

- [22] Zekovic S, Dwivedi R, Kovacevic R. Numerical simulation and experimental investigation of gas-powder flow from radially symmetrical nozzles in laser-based direct metal deposition. *Int J Mach Tools Manuf* 2007;47:112–23. doi:10.1016/j.ijmachtools.2006.02.004.
- [23] Lin J. Numerical simulation of the focused powder streams in coaxial laser cladding. *J Mater Process Technol* 2000;105:17–23. doi:10.1016/S0924-0136(00)00584-7.
- [24] Wen SY, Shin YC, Murthy JY, Sojka PE. Modeling of coaxial powder flow for the laser direct deposition process. *Int J Heat Mass Transf* 2009;52:5867–77. doi:10.1016/j.ijheatmasstransfer.2009.07.018.
- [25] Zhu G, Li D, Zhang A, Tang Y. Numerical simulation of metallic powder flow in a coaxial nozzle in laser direct metal deposition. *Opt Laser Technol* 2011;43:106–13. doi:10.1016/j.optlastec.2010.05.012.
- [26] Kovaleva I, Kovalev O, Zaitsev A, Smurov I. Numerical simulation and comparison of powder jet profiles for different types of coaxial nozzles in direct material deposition. *Phys Procedia* 2013;41:870–2. doi:10.1016/j.phpro.2013.03.160.
- [27] Smurov I, Doubenskaia M, Zaitsev A. Comprehensive analysis of laser cladding by means of optical diagnostics and numerical simulation. *Surf Coatings Technol* 2013;220:112–21. doi:10.1016/j.surfcoat.2012.10.053.
- [28] Ibarra-Medina J, Vogel M, Pinkerton AJ. A CFD model of laser cladding: From deposition head to melt pool dynamics. *Proc 30th Int Congr Appl Lasers Electro-Optics* 2011:378–86.

- [29] Devesse W, Baere D De, Guillaume P, Brussel VU. Modeling of Laser Beam and Powder Flow Interaction in Laser Cladding Using Ray-Tracing. *J Laser Appl* 2015;27:0–8. doi:10.2351/1.4906394.
- [30] Taberero I, Lamikiz A, Martínez S, Ukar E, López De Lacalle LN. Geometric modelling of added layers by coaxial Laser Cladding. *Phys Procedia* 2012;39:913–20. doi:10.1016/j.phpro.2012.10.116.
- [31] Liu CY, Lin J. Thermal processes of a powder particle in coaxial laser cladding. *Opt Laser Technol* 2003;35:81–6. doi:10.1016/S0030-3992(02)00145-7.
- [32] Kovalev OB, Kovaleva IO, Smurov IY. Numerical investigation of gas-disperse jet flows created by coaxial nozzles during the laser direct material deposition. *J Mater Process Technol* 2017;249:118–27. doi:10.1016/j.jmatprotec.2017.05.041.
- [33] Taberero I, Lamikiz A, Ukar E, Lopez De Lacalle LN, Angulo C, Urbikain G. Numerical simulation and experimental validation of powder flux distribution in coaxial laser cladding. *J Mater Process Technol* 2010;210:2125–34. doi:10.1016/j.jmatprotec.2010.07.036.
- [34] Wen S, Shin YC. Modeling of transport phenomena during the coaxial laser direct deposition process. *J Appl Phys* 2010;108:1–9. doi:10.1063/1.3474655.
- [35] Lin J. Laser attenuation of the focused powder streams in coaxial laser cladding. *J Laser Appl* 2000;12. doi:10.2351/1.521910.
- [36] Yang N. Concentration model based on movement model of powder flow in coaxial laser cladding. *Opt Laser Technol* 2009;41:94–8.

- doi:10.1016/j.optlastec.2008.03.008.
- [37] Pan H, Liou F. Numerical simulation of metallic powder flow in a coaxial nozzle for the laser aided deposition process. *Opt Laser Technol* 2011;43:106–13.  
doi:10.1016/j.jmatprotec.2004.11.017.
- [38] Zhang B, Coddet C. Numerical study on the effect of pressure and nozzle dimension on particle distribution and velocity in laser cladding under vacuum base on CFD. *J Manuf Process* 2016;23:54–60.  
doi:10.1016/j.jmapro.2016.05.019.
- [39] Tabernero I, Lamikiz A, Martínez S, Ukar E, López De Lacalle LN. Modelling of energy attenuation due to powder flow-laser beam interaction during laser cladding process. *J Mater Process Technol* 2012;212:516–22.  
doi:10.1016/j.jmatprotec.2011.10.019.
- [40] Liu J, Li L, Zhang Y, Xie X. Attenuation of laser power of a focused Gaussian beam during interaction between a laser and powder in coaxial laser cladding. *J Phys D Appl Phys* 2005;38:1546–50. doi:10.1088/0022-3727/38/10/008.
- [41] Kovaleva IO, Kovalev OB. Simulation of light-propulsion acceleration of powder particles for laser direct metal deposition. *Phys Procedia* 2011;12:285–95. doi:10.1016/j.phpro.2011.03.037.
- [42] Kovaleva IO, Kovalev OB. Simulation of the acceleration mechanism by light-propulsion for the powder particles at laser direct material deposition. *Opt Laser Technol* 2012;44:714–25. doi:10.1016/j.optlastec.2011.09.016.
- [43] Ibarra-Medina J, Pinkerton a. J. A numerical investigation of powder heating in

- coaxial laser direct metal deposition. 36th MATADOR Conf 2010;27:1–4.  
doi:10.1007/978-1-84996-432-6\_101.
- [44] Diniz Neto OO, Alcalde a. M, Vilar R. Interaction of a focused laser beam and a coaxial powder jet in laser surface processing. *J Laser Appl* 2007;19:84.  
doi:10.2351/1.2402523.
- [45] Wen S, Shin YC. Modeling of the Off-Axis High Power Diode Laser Cladding Process. *J Heat Transfer* 2011;133:31007. doi:10.1115/1.4002447.
- [46] Nie P, Ojo OA, Li Z. Modeling analysis of laser cladding of a nickel-based superalloy. *Surf Coatings Technol* 2014;258:1048–59.  
doi:10.1016/j.surfcoat.2014.07.030.
- [47] Balu P, Leggett P, Kovacevic R. Parametric study on a coaxial multi-material powder flow in laser-based powder deposition process. *J Mater Process Technol* 2012;212:1598–610. doi:10.1016/j.jmatprotec.2012.02.020.
- [48] Lee Y, Farson DF. Simulation of transport phenomena and melt pool shape for multiple layer additive manufacturing. *J Laser Appl* 2016;28:12006.  
doi:10.2351/1.4935711.
- [49] Cao Y, Choi J. Solidification Microstructure Evolution Model for Laser Cladding Process. *J Heat Transfer* 2007;129:852. doi:10.1115/1.2712856.
- [50] Qi H, Mazumder J, Ki H. Numerical simulation of heat transfer and fluid flow in coaxial laser cladding process for direct metal deposition. *J Appl Phys* 2006;100:1–11. doi:10.1063/1.2209807.
- [51] Picasso M, Hoadley AFA. Finite element simulation of Laser Surface

- Treatments including convection in the melt pool 1994;4:61–83.
- [52] Lee Y, Nordin M, Babu S, Farson D. Influence of Fluid Convection on Weld Pool Formation in Laser Cladding. *Weld J* 2014;93:292s–300s.
- [53] Kim J Do, Peng Y. Melt pool shape and dilution of laser cladding with wire feeding. *J Mater Process Technol* 2000;104:284–93. doi:10.1016/S0924-0136(00)00528-8.
- [54] Ya W, Pathiraj B, Liu S. 2D modelling of clad geometry and resulting thermal cycles during laser cladding. *J Mater Process Technol* 2016;230:217–32. doi:10.1016/j.jmatprotec.2015.11.012.
- [55] Han L, Phatak KM, Liou FW. Modeling of laser cladding with powder injection. *Metall Mater Trans B* 2004;35:1139–50. doi:10.1007/s11663-004-0070-0.
- [56] Choi J, Han L, Hua Y. Modeling and Experiments of Laser Cladding With Droplet Injection. *J Heat Transfer* 2005;127:978. doi:10.1115/1.2005273.
- [57] Chan C, Mazumder J, Chen MM. A two-dimensional transient model for convection in laser melted pool. *Metall Trans A* 1984;15:2175–84. doi:10.1007/BF02647100.
- [58] Kong F, Kovacevic R. Modeling of heat transfer and fluid flow in the laser multilayered cladding process. *Metall Mater Trans B Process Metall Mater Process Sci* 2010;41:1310–20. doi:10.1007/s11663-010-9412-2.
- [59] Mirzade FK, Niziev VG, Panchenko VY, Khomenko MD, Grishaev R V., Pityana S, et al. Kinetic approach in numerical modeling of melting and crystallization at laser cladding with powder injection. *Phys B Condens Matter*

- 2013;423:69–76. doi:10.1016/j.physb.2013.04.053.
- [60] Esmaeelpanah J, Passandideh-Fard M. On a Numerical Model of Laser Cladding Process. Proc. 14th Int. Heat Transf. Conf. IHTC14, Washington, DC, USA: 2010, p. 1–8.
- [61] Morville S, Carin M. 2D longitudinal modeling of heat transfer and fluid flow during multilayered direct laser metal deposition process. J Laser Appl 2012;24:1–4. doi:10.2351/1.4726445.
- [62] Kumar A, Roy S. Effect of three-dimensional melt pool convection on process characteristics during laser cladding. Comput Mater Sci 2009;46:495–506. doi:10.1016/j.commatsci.2009.04.002.
- [63] Hao M, Sun Y. A FEM model for simulating temperature field in coaxial laser cladding of Ti6Al4V alloy using an inverse modeling approach. Int J Heat Mass Transf 2013;64:352–60. doi:10.1016/j.ijheatmasstransfer.2013.04.050.
- [64] Guo LF, Yue TM, Man HC. A finite element method approach for thermal analysis of laser cladding of magnesium alloy with preplaced Al–Si powder. J Laser Appl 2004;16:229. doi:10.2351/1.1809634.
- [65] Lei Y, Sun R, Tang Y, Niu W. Numerical simulation of temperature distribution and TiC growth kinetics for high power laser clad TiC/NiCrBSiC composite coatings. Opt Laser Technol 2012;44:1141–7. doi:10.1016/j.optlastec.2011.09.030.
- [66] Yevko V, Park CB, Zak G, Coyle TW, Benhabib B. Cladding formation in laser-beam fusion of metal powder. Universi of Toronto, 1998.

doi:10.1108/13552549810239021.

- [67] Gouge MF, Heigel JC, Michaleris P, Palmer TA. Modeling forced convection in the thermal simulation of laser cladding processes. *Int J Adv Manuf Technol* 2015;307–20. doi:10.1007/s00170-015-6831-x.
- [68] Luo F, Yao J, Hu X, Chai G. Effect of Laser Power on the Cladding Temperature Field and the Heat Affected Zone. *J Iron Steel Res Int* 2011;18:73–8. doi:10.1016/S1006-706X(11)60014-9.
- [69] Hoadley AFA, Rappaz M. A Thermal Model of Laser Cladding by Powder Injection. *Metall Trans B* 1992;23B:631–42.
- [70] Toyserkani E, Khajepour A, Corbin S. 3-D finite element modeling of laser cladding by powder injection: Effects of laser pulse shaping on the process. *Opt Lasers Eng* 2004;41:849–67. doi:10.1016/S0143-8166(03)00063-0.
- [71] Huang YL, Liu J, Ma NH, Li J-G. Three-dimensional analytical model on laser-powder interaction during laser cladding. *J Laser Appl* 2006;18:42. doi:10.2351/1.2164476.
- [72] Alimardani M, Toyserkani E, Huissoon JP. A 3D dynamic numerical approach for temperature and thermal stress distributions in multilayer laser solid freeform fabrication process. *Opt Lasers Eng* 2007;45:1115–30. doi:10.1016/j.optlaseng.2007.06.010.
- [73] Cheikh H El, Courant B. 3D Finite Element Simulation to Predict the Induced Thermal Field in Case of Laser Cladding Process and Half Cylinder Laser Clad 2012;1:55–9.

- [74] Lei Y, Sun R, Lei J, Tang Y, Niu W. A new theoretical model for high power laser clad TiC/NiCrBSiC composite coatings on Ti6Al4V alloys. *Opt Lasers Eng* 2010;48:899–905. doi:10.1016/j.optlaseng.2010.03.016.
- [75] Kaplan AFH, Groboth G. Process Analysis of Laser Beam Cladding. *J Manuf Sci Eng* 2001;123:609. doi:10.1115/1.1344899.
- [76] Tseng WC, Aoh JN. Simulation study on laser cladding on preplaced powder layer with a tailored laser heat source. *Opt Laser Technol* 2013;48:141–52. doi:10.1016/j.optlastec.2012.09.014.
- [77] Yong Y, Fu W, Deng Q, Chen D. A comparative study of vision detection and numerical simulation for laser cladding of nickel-based alloy. *J Manuf Process* 2017;28:364–72. doi:10.1016/j.jmapro.2017.03.004.
- [78] Parekh R, Buddu RK, Patel RI. Multiphysics simulation of laser cladding process to study the effect of process parameters on clad geometry. *Procedia Technol* 2016;23:529–36. doi:10.1016/j.protcy.2016.03.059.
- [79] Farahmand P, Kovacevic R. Laser cladding assisted with an induction heater (LCAIH) of Ni-60%WC coating. *J Mater Process Technol* 2015;222:244–58. doi:10.1016/j.jmatprotec.2015.02.026.
- [80] Farahmand P, Kovacevic R. An experimental–numerical investigation of heat distribution and stress field in single- and multi-track laser cladding by a high-power direct diode laser. *Opt Laser Technol* 2014;63:154–68. doi:10.1016/j.optlastec.2014.04.016.
- [81] He X, Yu G, Mazumder J. Temperature and composition profile during double-

- track laser cladding of H13 tool steel. *J Phys D Appl Phys* 2010;43.  
doi:10.1088/0022-3727/43/1/015502.
- [82] Liu H, Qin X, Huang S, Hu Z, Ni M. Geometry modeling of single track cladding deposited by high power diode laser with rectangular beam spot. *Opt Lasers Eng* 2018;100:38–46. doi:10.1016/j.optlaseng.2017.07.008.
- [83] Bedenko D V., Kovalev OB, Smurov I, Zaitsev A V. Numerical simulation of transport phenomena, formation the bead and thermal behavior in application to industrial DMD technology. *Int J Heat Mass Transf* 2016;95:902–12.  
doi:10.1016/j.ijheatmasstransfer.2015.12.046.
- [84] Lin J, Steen WM. An in-process method for the inverse estimation of the powder catchment efficiency during laser cladding. *Opt Laser Technol* 1998;30:77–84. doi:10.1016/S0030-3992(98)00007-3.
- [85] Zeinali M, Khajepour A. Development of an adaptive fuzzy logic-based inverse dynamic model for laser cladding process. *Eng Appl Artif Intell* 2010;23:1408–19. doi:10.1016/j.engappai.2009.11.006.
- [86] Chande T, Mazumder J. Two-Dimensional, Transient Model for Mass-Transport in Laser Surface Alloying. *J Appl Phys* 1985;57:2226–32.  
doi:10.1063/1.334367.
- [87] Palumbo G, Pinto S, Tricarico L. Numerical finite element investigation on laser cladding treatment of ring geometries. *J Mater Process Technol* 2004;155–156:1443–50. doi:10.1016/j.jmatprotec.2004.04.360.
- [88] Raju R, Petley V, G. K. A, Duraiselvam M, Verma S, Rajendran R. Numerical

- finite element investigation on Laser Cladding of aerospace components. *Life Cycle Reliab Saf Eng* 2014;3:13–23.
- [89] Lee YS, Zhang W. Modeling of heat transfer, fluid flow and solidification microstructure of nickel-base superalloy fabricated by laser powder bed fusion. *Addit Manuf* 2016;12:178–88. doi:10.1016/j.addma.2016.05.003.
- [90] Masoomi M, Thompson SM, Shamsaei N. Laser powder bed fusion of Ti-6Al-4V parts: Thermal modeling and mechanical implications. *Int J Mach Tools Manuf* 2017;118–119:73–90. doi:10.1016/j.ijmachtools.2017.04.007.
- [91] Nazemi N, Urbanic RJ. A numerical investigation for alternative toolpath deposition solutions for surface cladding of stainless steel P420 powder on AISI 1018 steel substrate. *Int J Adv Manuf Technol* 2018;96:4123–43. doi:10.1007/s00170-018-1840-1.
- [92] Song L, Bagavath-Singh V, Dutta B, Mazumder J. Control of melt pool temperature and deposition height during direct metal deposition process. *Int J Adv Manuf Technol* 2012;58:247–56. doi:10.1007/s00170-011-3395-2.
- [93] Kohler H, Thomy C, Vollertsen F. Contact-less temperature measurement and control with applications to laser cladding. *Weld World* 2016;60:1–9. doi:10.1007/s40194-015-0275-7.
- [94] Tran HS, Tchuindjang JT, Paydas H, Mertens A, Jardin RT, Duchêne L, et al. 3D thermal finite element analysis of laser cladding processed Ti6Al4V part with microstructural correlations. *Mater Des* 2017;128:130–42. doi:10.1016/j.matdes.2017.04.092.

- [95] Suarez A, Tobar MJ, Yaez A, Perez I, Sampedro J, Amigo V, et al. Modeling of phase transformations of Ti6Al4V during laser metal deposition. *Phys Procedia* 2011;12:666–73. doi:10.1016/j.phpro.2011.03.083.
- [96] Kongsuwan P, Brandal G, Lawrence Yao Y. Laser Induced Porosity and Crystallinity Modification of a Bioactive Glass Coating on Titanium Substrates. *J Manuf Sci Eng* 2015;137:31004. doi:10.1115/1.4029566.
- [97] Lee Y, Nordin M, Babu SS, Farson DF. Effect of fluid convection on dendrite arm spacing in laser deposition. *Metall Mater Trans B Process Metall Mater Process Sci* 2014;45:1520–9. doi:10.1007/s11663-014-0054-7.
- [98] Gao W, Zhao S, Wang Y, Zhang Z, Liu F, Lin X. Numerical simulation of thermal field and Fe-based coating doped Ti. *Int J Heat Mass Transf* 2016;92:83–90. doi:10.1016/j.ijheatmasstransfer.2015.08.082.
- [99] Farahmand P, Balu P, Kong F, Kovacevic R. Investigation of Thermal Cycle and Hardness Distribution in the Laser Cladding of AISI H13 tool steel produced by a High Power Direct Diode Laser. *Proc. ASME 2013 Int. Mech. Eng. Congr. Expo., Callifornia, USA: 2015*, p. 1–12.
- [100] Santhanakrishnan S, Kong F, Kovacevic R. An experimentally based thermo-kinetic hardening model for high power direct diode laser cladding. *J Mater Process Technol* 2011;211:1247–59. doi:10.1016/j.jmatprotec.2011.02.006.
- [101] Gu S, Chai G, Wu H, Bao Y. Characterization of local mechanical properties of laser-cladding H13-TiC composite coatings using nanoindentation and finite element analysis. *Mater Des* 2012;39:72–80. doi:10.1016/j.matdes.2012.02.028.

- [102] Suarez A, Amado JM, Tobar MJ, Yanez A, Fraga E, Peel MJ. Study of residual stresses generated inside laser clad plates using FEM and diffraction of synchrotron radiation. *Surf Coatings Technol* 2010;204:1983–8. doi:10.1016/j.surfcoat.2009.11.037.
- [103] Deus A, .M., Mazumder J. Three-dimensional finite element models for the calculation of temperature and residual stress fields in laser cladding. *Arbor* 2006;1001:48109.
- [104] Moat RJ, Pinkerton AJ, Li L, Withers PJ, Preuss M. Residual stresses in laser direct metal deposited Waspaloy. *Mater Sci Eng A* 2011;528:2288–98. doi:10.1016/j.msea.2010.12.010.
- [105] Plati A, Tan JC, Golosnoy IO, Persoons R, Van Acker K, Clyne TW. Residual stress generation during laser cladding of steel with a particulate metal matrix composite. *Adv Eng Mater* 2006;8:619–24. doi:10.1002/adem.200600063.
- [106] Paul S, Ashraf K, Singh R. Residual stress modeling of powder injection laser surface cladding for die repair applications. *ASME 2014 Int Manuf Sci Eng Conf MSEC 2014 Collocated with JSME 2014 Int Conf Mater Process 42nd North Am Manuf Res Conf* 2014;2:1–8. doi:10.1115/MSEC2014-4029.
- [107] Bailey NS, Katinas C, Shin YC. Laser direct deposition of AISI H13 tool steel powder with numerical modeling of solid phase transformation, hardness, and residual stresses. *J Mater Process Technol* 2017;247:223–33. doi:10.1016/j.jmatprotec.2017.04.020.
- [108] Alam MM, Kaplan AFH, Tuominen J, Vuoristo P, Miettinen J, Poutala J, et al. Analysis of the stress raising action of flaws in laser clad deposits. *Mater Des*

- 2013;46:328–37. doi:10.1016/j.matdes.2012.10.010.
- [109] Paul S, Thool K, Singh R, Samajdar I, Yan W. Experimental Characterization of Clad Microstructure and its Correlation with Residual Stresses. *Procedia Manuf* 2017;0:804–18. doi:10.1016/j.promfg.2017.07.081.
- [110] Jiang W, Liu Z, Gong JM, Tu ST. Numerical simulation to study the effect of repair width on residual stresses of a stainless steel clad plate. *Int J Press Vessel Pip* 2010;87:457–63. doi:10.1016/j.ijpvp.2010.06.003.
- [111] Brückner F, Lepski D, Beyer E. Modeling the Influence of Process Parameters and Additional Heat Sources on Residual Stresses in Laser Cladding. *J Therm Spray Technol* 2007;16:355–73. doi:10.1007/s11666-007-9026-7.
- [112] Krzyzanowski M, Bajda S, Liu Y, Triantaphyllou A, Rainforth WM, Glendenning M, et al. 3D analysis of thermal and stress evolution during laser cladding of bioactive glass coatings. *J Mech Behav Biomed Mater* 2016;59:404–17. doi:10.1016/j.jmbbm.2016.02.023.
- [113] Chew Y, Pang JHL. Fatigue life prediction model for laser clad AISI 4340 specimens with multiple surface cracks. *Int J Fatigue* 2016;87:235–44. doi:10.1016/j.ijfatigue.2016.01.025.
- [114] Paul S, Gupta I, Singh RK. Characterization and Modeling of Microscale Preplaced Powder Cladding Via Fiber Laser. *J Manuf Sci Eng* 2015;137:31019. doi:10.1115/1.4029922.
- [115] Additive Manufacturing, Loughborough University n.d. <https://www.lboro.ac.uk/research/amrg/about/the7categoriesofadditivemanufac>

turing/ (accessed April 26, 2019).

- [116] 3D HUBS n.d. <https://www.3dhubs.com/knowledge-base/additive-manufacturing-technologies-overview> (accessed April 26, 2019).
- [117] Du W. IMECE2017-70344 BINDER JETTING ADDITIVE MANUFACTURING OF CERAMICS : A LITERATURE 2018:1–12.
- [118] Gonzalez-Gutierrez J, Cano S, Schuschnigg S, Kukla C, Sapkota J, Holzer C. Additive Manufacturing of Metallic and Ceramic Components by the Material Extrusion of Highly-filled Polymers A Review and Future Perspectives n.d. doi:10.3390/ma11050840.
- [119] Dilag J, Chen T, Li S, Bateman SA. Design and direct additive manufacturing of three-dimensional surface micro-structures using material jetting technologies. *Addit Manuf* 2019;27:167–74. doi:10.1016/j.addma.2019.01.009.
- [120] Hafkamp T, Baars G Van, Jager B De, Etman P. A feasibility study on process monitoring and control in vat photopolymerization of ceramics. *Mechatronics* 2018;56:220–41. doi:10.1016/j.mechatronics.2018.02.006.
- [121] Bhatt PM, Kabir AM, Peralta M, Bruck HA, Gupta SK. A robotic cell for performing sheet lamination-based additive manufacturing. *Addit Manuf* 2019;27:278–89. doi:10.1016/j.addma.2019.02.002.
- [122] Haridas A, Vadakke M, Crivoi A, Patinharekandy P, Ming T, Chan K. Surface roughness evaluation of additive manufactured metallic components from white light images captured using a flexible fiberscope. *Opt Lasers Eng* 2018;110:262–71. doi:10.1016/j.optlaseng.2018.05.026.

- [123] Donadello S, Motta M, Demir AG, Previtali B. Monitoring of laser metal deposition height by means of coaxial laser triangulation 2019;112:136–44. doi:10.1016/j.optlaseng.2018.09.012.
- [124] Ni C, Shi Y, Liu J, Huang G. Characterization of Al<sub>0.5</sub>FeCu<sub>0.7</sub>NiCoCr high-entropy alloy coating on aluminum alloy by laser cladding. Opt Laser Technol 2018;105:257–63. doi:10.1016/j.optlastec.2018.01.058.
- [125] Jiang D, Hong C, Zhong M, Alkhayat M, Weisheit A, Gasser A, et al. Fabrication of nano-TiCp reinforced Inconel 625 composite coatings by partial dissolution of micro-TiCp through laser cladding energy input control. Surf Coat Technol 2014;249:125–31. doi:10.1016/j.surfcoat.2014.03.057.
- [126] Torres JMSP, Leonor T, Morgado M, Navas H. Innovative Automation Equipment of Laser Cladding 2015. doi:10.13140/RG.2.1.3675.4002.
- [127] Laser Cladding System Market Outlook n.d. <https://businessherald.co/tag/laser-cladding-system-market-outlook/> (accessed April 26, 2019).
- [128] Wang D, Hu Q, Zheng Y, Xie Y, Zeng X. Study on deposition rate and laser energy efficiency of Laser-Induction Hybrid Cladding. Opt Laser Technol 2016;77:16–22. doi:10.1016/j.optlastec.2015.08.019.
- [129] Li M, Han B, Wang Y, Song L, Guo L. Investigation on laser cladding high-hardness nano-ceramic coating assisted by ultrasonic vibration processing. Opt - Int J Light Electron Opt 2016;127:4596–600. doi:10.1016/j.ijleo.2016.01.194.

- [130] Davim JP, Oliveira C, Cardoso A. Predicting the geometric form of clad in laser cladding by powder using multiple regression analysis ( MRA ) 2008;29:554–7. doi:10.1016/j.matdes.2007.01.023.
- [131] Fu Y, Loredo A, Martin B, Vannes AB. A theoretical model for laser and powder particles interaction during laser cladding 2002;128:106–12.
- [132] Tamanna N, Crouch R, Kabir IR, Naher S. An analytical model to predict and minimize the residual stress of laser cladding process. Appl Phys A Mater Sci Process 2018;124:0. doi:10.1007/s00339-018-1585-6.

## List of Figures

Fig. 1 Schematic diagrams of feeding system (a) preplaced powder system, (b) co-axial powder system, (c) off-axis powder system and (d) wire feeding system. ....	4
Fig. 2 (a) A schematic diagram of the coaxial Laser Cladding process, (b) micrograph, presenting deposited clad, HAZ and substrate area [17]......	5
Fig. 3 Schematic diagram of several interaction zones along the laser beam to substrate. The interactions can be divided into three zones such as (a) powder-nozzle [34,39], (b) powder-laser [22,39,41,43]and (c) powder-substrate [22]. LFD = laser focus distance, SOD = stand of distance, BOE = bounce off effect.....	9
Fig. 4 The categories of additive manufacturing technology based on materials and machine technology[115,116]. ....	33
Fig. 5 Available models of the Laser Cladding process can be applied for additive manufacturing. ....	36

## List of Tables

Table 1: The chronological development of numerical models on powder flow dynamics for co-axial powder type. ....	13
Table 2. Chronological development of thermal model in melt pool .....	23